Computers & Geosciences 91 (2016) 105–118

Contents lists available at ScienceDirect

Computers & Geosciences

journal homepage: www.elsevier.com/locate/cageo

Research paper

Migration tracing and kinematic state concept embedded in discrete fracture network for modeling hydrocarbon migration around unlined rock caverns

Morteza Javadi, Mostafa Sharifzadeh *[,1], Kourosh Shahriar, Shahrbanou Sayadi

Department of Mining & Metallurgical Engineering, Amirkabir University of Technology, Hafez 424, Tehran 15875-4413, Iran

ARTICLE INFO

Article history:
Received 10 February 2015
Received in revised form
13 February 2016
Accepted 15 February 2016
Available online 16 February 2016

Keywords:
DFN
Unlined rock cavern
Hydrocarbon migration
Tracing algorithm
Hydraulic confinement

ABSTRACT

This paper presents a numerical method for the modeling of hydraulic confinement and hydrocarbon migration around the unlined rock caverns (URCs) by directly applying distinct fracture network (DFN) concept. A "migration tracing" algorithm for the assessment of hydrocarbon migration around URCs was developed based on the applying migration cessation criterion and pathway analysis in the DFN realizations. The veracity of the developed numerical method was explored by predicting the hydrocarbon migration in a uniform fracture network around an unlined cavern that consists with results obtained from the finite element continuum fluid flow analysis. Finally, the applicability of the proposed method was evaluated by simulation of hydrocarbon migration in the DFN realizations around a URC. The results demonstrate that the hydrocarbon migration is sensitive to the hydraulic boundary conditions, and the geometrical properties of fractures. Establishing sufficient water pressure in the fracture system controls hydrocarbon migration; however, the effect of external water pressure on the hydrocarbon migration is controlled by the fractures geometry. Consequently, local migration paths may develop around storage caverns through the intricately connected fracture network, despite the presence of high pressurized water curtain. The proposed method may prove useful for better design analysis of hydraulic confinement around URCs, or inclusions in simulators for computational demands.

1. Introduction

Prediction of environmental impacts and the efficiency of hydraulic confinement for hydrocarbon storage in unlined rock caverns (URCs) are the most critical issues faced by Hydrogeologists. Successful prediction of such issues requires realistic and robust predictive models based on the physical processes that govern fluid flow in rock mass.

The typical safety concern in URCs is to prevent hydrocarbon leakage from the cavern to the surrounding rock mass. The principle behind prevention of hydrocarbon leakage in URCs, called hydraulic confinement, is based on the application of groundwater pressure on the surrounding rock to confine the stored hydrocarbon inside the caverns (Froise, 1987). Appropriate application of hydraulic confinement poses a key question; (Liang and Lindblom, 1994; Chung et al., 2003); How large of pressure difference between groundwater and stored hydrocarbon in the cavern should be maintained to prevent hydrocarbon leakage?

The exact criterion for preventing hydrocarbon leakage from the URCs has been a matter of research for several years. During the past decades, different gas-containment, no gas leakage, criteria have been proposed based on groundwater gradient or pressure (Åberg, 1977; Goodall et al., 1988; Liang and Lindblom, 1994; Lindblom, 1997) that are theoretically a priority. These hydraulic criteria have been mostly applied in continuum numerical modeling efforts (Thunvik and Braester, 1981; Chung et al., 2003; Kim et al., 2007; Maejima et al., 2007; Aoki et al., 2010; Sun and Zhao, 2010). However, most of the URCs are constructed in good quality and hard rocks (Froise, 1987; Zhao, 1996; Lee and Song, 2003), where fractures are the main flow paths and control the hydrocarbon leakage phenomenon (Goel et al., 2012; Yoshida et al., 2013). In fact, the physical processes that govern hydraulic behavior of rock mass are significantly controlled by the fractures (Indraratna et al., 1999, 2003; Javadi et al., 2010, 2014, 2015). In such situation, discontinuum representations of fractured rock,

* Corresponding author.
E-mail addresses: ttscopo@aut.ac.ir (M. Javadi), shariszadeh@aut.ac.ir, M.Sharifzadeh@curtin.edu.au (M. Sharifzadeh), k.shahriar@aut.ac.ir (K. Shahriar), a_sayadi@rocketmail.com (S. Sayadi).
[1] Western Australian School of Mine (WASM), Curtin University, Western Australia, Australia.

http://dx.doi.org/10.1016/j.cageo.2016.02.012
0098-3004/

such as discrete fracture network (DFN) concept, appear much more adapted to physical processes. However, only a few studies (Dershowitz and Lapointe, 1995; Ra and Sung, 1999; Lee and Song, 2003) have been implemented on the fluid flow analysis in the rock mass surrounding the URCs via direct utilization of DFN. Dershowitz and Lapointe (1995) used a combination of DFN and percolation theory to evaluate the probability of gas escape (a percolation problem). Ra and Sung (1999) utilized a flow simulator in DFN to investigate the distribution of hydraulic head around a URC. The result of these studies showed that the discrete fracture model is more appropriate for the analysis of groundwater flow than the continuum model. A similar attempt was reported by Lee and Song (2003). Although the above-mentioned researches improved the general knowledge about the circumstances related to fluid flow around the URCs, a few studies have been focused on the numerical modeling of hydrocarbon migration. Moreover, few efforts have been implemented on the numerical modeling of hydrocarbon migration from the URCs to surrounding rock mass via direct utilization of DFN concept. Due to the destructive environmental consequences of hydrocarbon leakage, a more efficient and reliable model is strongly required for analysis of water-hydrocarbon interaction through the fractured rock mass surrounding the URCs that is developed and illustrated in this paper.

The purpose of this study is to develop a more realistic numerical method for modeling the hydrocarbon migration from URCs. For this purpose, an algorithm including new concepts, so-called "migration tracing" and "kinematic state", was developed based on the pathway analysis in the DFN and applying the migration cessation criterion. These procedures were integrated into the "FNETF" computational code, previously developed and validated for fluid flow analysis in fractured rocks (Javadi and Sharifzadeh, 2011a, 2011b, 2014; Sharifzadeh and Javadi, 2011; Javadi et al., 2016). The accuracy of the developed algorithm and numerical method was explored by predicting the hydrocarbon migration in a uniform fractured rock around an unlined cavern and comparing it with the results of finite element continuum fluid flow analysis. Finally, the procedure for hydrocarbon migration was numerically investigated in two different DFN realizations to evaluate the applicability of the developed numerical method for naturally fractured rock mass.

2. Concepts and theoretical background

2.1. Hydraulic confinement

The methods for limiting or eliminating hydrocarbon leakage from rock caverns can be categorized based on two main principles of permeability control, and hydraulic confinement (Kjørholt and Broch, 1992; Lu, 2010). Permeability control means that the leakage is eliminated by excavating the cavern in natural tight rocks (such as salt beds) or by using extra supplementary lining that refer to lined rock cavern. The second principle or "hydraulic confinement" is based on the application of groundwater pressure in the surrounding rock to confine the stored hydrocarbon inside the caverns. The technique of hydraulic confinement is to establish continuous groundwater flow toward the cavern from outside rock to prevent the hydrocarbon migration. To achieve the hydraulic confinement, the actual groundwater pressure acting on the cavern periphery should exceed the vapor pressure of the hydrocarbon by a certain amount.

Prevention of leakage by hydraulic confinement offers two alternatives: (1) natural groundwater pressure supplied by natural sources such as lake or sea; and (2) artificial water supply that is provided by installing so-called "water curtain" outside the cavern periphery. The groundwater pressure will drop if water is continuously removed from the cavern without sufficient natural replenishment (Thunvik and Braester, 1981). In most cases, the sufficient replenishment and necessary groundwater pressure can only be artificially achieved by installing water curtain. The water curtain installation consists of some infiltration galleries located above the caverns and arrays of boreholes drilled from these galleries (Fig. 1). The infiltration galleries will be filled and fed with pressurized water to supply the boreholes. The water is permanently injected to ensure full water saturation of rock in the construction and utilization phases. The water leaking into the cavern forms a layer, so-called water bed, on the cavern floor. The hydrocarbon products float freely on the water bed, because they are lighter and also insoluble in water. The leaking water is collected in a sump excavated in the cavern floor and pumped out (from sump) continuously to maintain the water bed in a constant level near the cavern floor. Pumping out the leaking water and feeding the infiltration gallery with external supply remain the system in a stable hydraulic state in the operation phase.

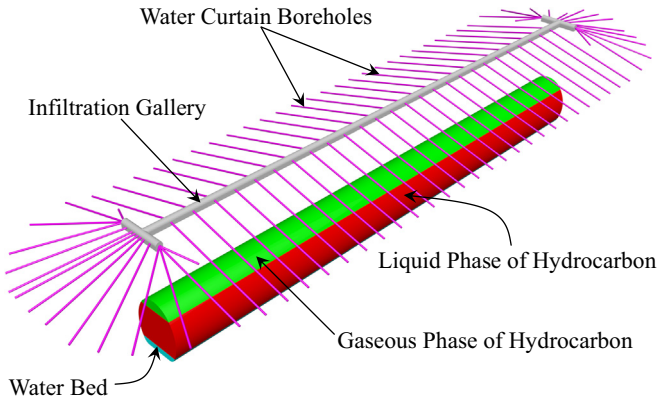

Fig. 1. Installation and components of water curtain around an unlined storage cavern.

2.2. Migration cessation criterion

Physically speaking, hydrocarbon migration from URCs is only possible along the fractures that provide declining hydrodynamic pressure away from the cavern (Goel et al., 2012). The hydrocarbon leakage phenomenon can be divided into two different physical processes. The first process is "hydrocarbon entry" from the storage into the rock fracture entrance that occurs when the hydrocarbon capillary force exceeds the pressure difference across the fracture interface within the cavern. The second process refers to the further movement of entering hydrocarbon along the fractures that called "hydrocarbon migration" (Åberg, 1977). Since the hydrocarbon entry is a very complicated physical process and very sensitive to high uncertain factors such as fracture-cavern intersection geometry, distribution of capillary force, and pressure distribution across the fracture interface, this process is rarely considered in practical design. In fact, most practical design approach for URCs is the prevention of hydrocarbon migration, not the entry (Söder, 1995). Therefore, the numerical method developed in this paper mainly focuses on the hydrocarbon migration process.

The hydrocarbon migration mostly occurs in the form of bubbles moving upward through the fracture (in the opposite direction of downward water flow). A schematic view of the forces acting on a hydrocarbon bubble in water-filled fracture (with downward water flow) is shown in Fig. 2. These forces are weight of the bubble, F_G, capillary force, F_C, and hydraulic pressure, p_w. The necessary condition to prevent the upward movement of hydrocarbon bubble along the fractures (for two-dimensional cases) can

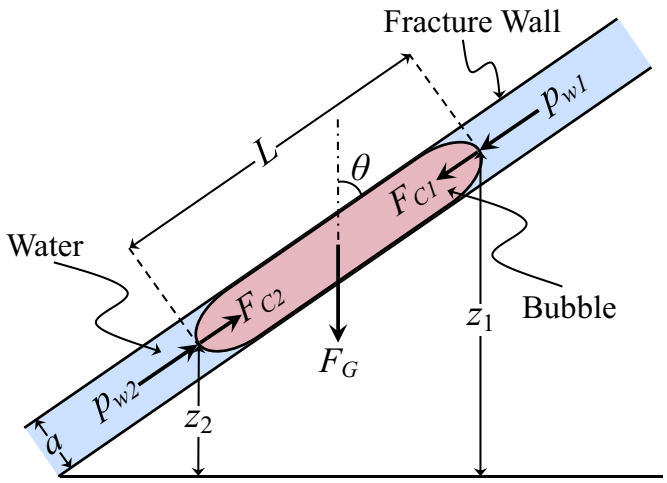

Fig. 2. A schematic view of forces acting on a hydrocarbon bubble in water-filled fracture.

be expressed by (Kim et al., 2000)

$$ap_{w1}+F_{C1}+F_G\cos\theta \geq ap_{w2}+F_{C2}, \tag{1}$$

where a is the aperture of the idealized smooth fracture. The bubble weight (F_G) can be calculated as

$$F_G=\rho_h gLa, \tag{2}$$

where ρ_h is the hydrocarbon density, g is the gravity acceleration, and L is the bubble length. By substituting Eq. (2) into Eq. (1), the rearranged form of migration cessation criterion can be written as,

$$(p_{w1}-p_{w2})+\frac{(F_{C1}-F_{C2})}{a} \geq -\rho_h gL\cos\theta. \tag{3}$$

At any arbitrary point along the flow streamline, the total head or energy head (H^T) is described by

$$H^T=z+\frac{p}{\rho g}+\frac{v^2}{2g}, \tag{4}$$

where the elevation of the point from a reference plane, p is the pressure at the chosen point, and v is the fluid velocity. The decrease of total head, ΔH^T, between the points (1) and (2) in the Fig. 2 can be written as

$$\Delta H^T=(H_1^T-H_2^T)=(z_1-z_2)+\left(\frac{p_{w1}-p_{w2}}{\rho_w g}\right)+\left(\frac{v_1^2-v_2^2}{2g}\right), \tag{5}$$

where ρ_w is the density of water. Substituting Eq. (5) into Eq. (3) leads to,

$$\Delta H^T \geq (z_1-z_2)-\frac{\rho_h}{\rho_w}L\cos(\theta)+\left(\frac{v_1^2-v_2^2}{2g}\right)-\left(\frac{F_{C1}-F_{C2}}{ag\rho_w}\right). \tag{6}$$

By neglecting the last two terms (velocity and capillary force differences) in Eq. (6), the migration cessation criterion can be formulated as,

$$\Delta H^T \geq \left[1-\frac{\rho_h}{\rho_w}\right](z_1-z_2), \tag{7-a}$$

$$\Delta H^T \geq \left[1-\frac{\rho_h}{\rho_w}\right]L\cos(\theta). \tag{7-b}$$

3. Development of numerical method

3.1. DFN generation and regularization

The DFN concept, in which the rock is considered as a network of individual interconnected fractures, is an alternative to discontinuum representation of fractured rocks. The DFN concept is introduced as a practical tool for analyzing fluid flow in fractured rocks due to the detailed geometrical description of the fractures.

The "FNETF" computational code, utilized in this study, uses the Monte Carlo method to generate two-dimensional DFN realizations based on the geometrical properties of fractures. Two-dimensional fracture system is created in an area called generation region (Fig. 3). After the generation of all fractures, a flow domain within the generation region is selected for fluid flow analysis. The underground excavation boundaries are also generated through the flow domain. Fractures crossing the boundaries, flow domain or excavation, are truncated and the hydraulically inactive fractures are deleted and the "dead-ends" of the interconnected fractures are removed. These two steps refer to DFN regularization. A schematic view of the procedures involved in the generation and regularization of a DFN realization is shown in Fig. 3.

3.2. Fluid flow analysis

After DFN generation and regularization, the fluid flow equations can be numerically solved through the regularized realization. This procedure is usually performed by converting the regularized DFN realization to a computational domain of nodes and elements consisting of fracture intersections and fracture segments between nodes, respectively. The nodes in the computational domain can be categorized into boundary and internal nodes in which the hydraulic head are known and unknown, respectively. The hydraulic head at each internal nodes and flow rate in each elements are calculated using a flow network technique, by establishing cubic law (Witherspoon et al., 1980) and mass continuity equations. A more generalized and modified form of cubic law, which can be applied to natural fractures, can be expressed as (Renshaw, 1995)

$$Q_{ij}=\frac{\gamma w a_h^3}{12\mu}\frac{(H_i-H_j)}{L_{ij}}=C_{ij}(H_i-H_j), \tag{8}$$

where Q_{ij} is the total volumetric flow rate through the fracture segment between nodes i and j (flow from i to j), μ is the fluid viscosity, γ is the fluid weight density, H_i is the hydraulic head (the sum of elevation and pressure head) at node i, L_{ij} is the length of fracture segment, w is the fracture width perpendicular to the pressure gradient, a_h is the hydraulic aperture, and C_{ij} is the conductance ratio of fracture.

In order to achieve a closed system for steady state flow condition, the continuity equation, which represents conservation of mass, should be applied for all internal and boundary nodes. For an incompressible fluid (i.e. water), conservation of mass is equivalent to conservation of volume. Here, a convention is used indicating that flow to the node is positive and flow out is negative. For j-th internal node, the continuity equation can be expressed by

$$\sum_{i=1}^{n_c} Q_{ij}=\sum_{i=1}^{n_c} C_{ij}(H_i-H_j)=0, \tag{9}$$

where n_c is the number of fracture segments intersecting at node j. From this equation, the unknown hydraulic head at node j can be calculated as (Priest, 1993)

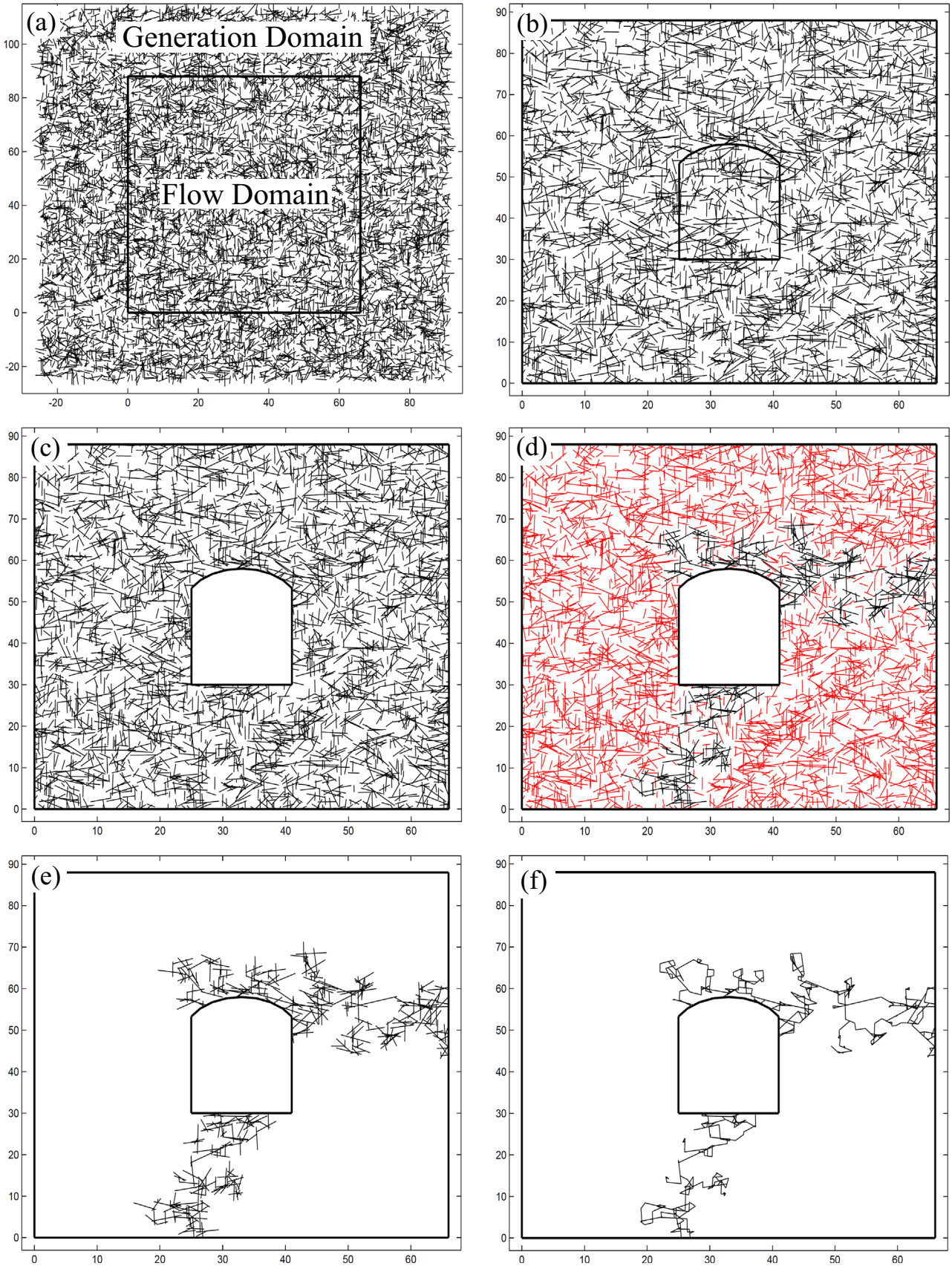

Fig. 3. Procedure for generation and regularization of DFN realization around an underground excavation: (a) generation region, (b) truncation of fractures crossing flow domain boundaries and generation of excavation or internal boundaries, (c) removing fractures inside the excavation and truncation of fractures crossing excavation boundaries, (d) finding the hydraulically inactive fractures, (e) removing the hydraulically inactive fractures, and (f) removing the blind or "dead-ends" of the interconnected fractures.

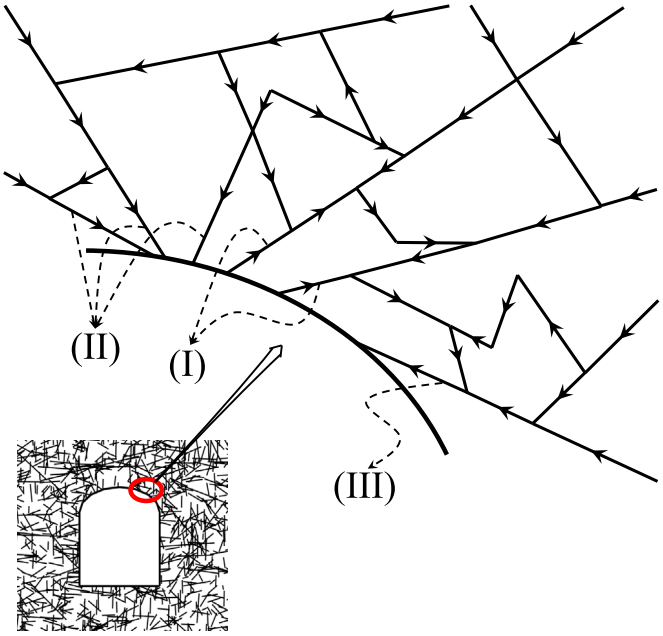

Fig. 4. Different kinematic states of fractures directly connected to the cavern boundary including outward flow (I), simultaneous inward and downward flow (II), and simultaneous inward and upward flow (III).

$$H_j = \frac{\sum_{i=1}^{n_c} C_{ij} H_i}{\sum_{i=1}^{n_c} C_{ij}} = \frac{\sum_{i=1}^{n_c} C_{ij} H_i}{C_j^s}, \tag{10}$$

where the term C_j^s represents the summation of conductance of all the fracture segments meeting at node j. Here, the conductance of each fracture segments meeting the node j can be normalized with C_j^s as

$$d_{ij} = \frac{C_{ij}}{C_j^s}, \tag{11}$$

where d_{ij} is the normalized conductance of i-th fracture segment meeting the node j. Using the normalized conductance of fracture segments, Eq. (10) can be reformulated as (Priest, 1993)

$$H_j = \frac{\sum_{i=1}^{n_c} C_{ij} H_i}{C_j^s} = \sum_{i=1}^{n_c} (d_{ij} H_i), \tag{12-a}$$

$$\sum_{i=1}^{n_c} (d_{ij} H_i) - H_j = 0. \tag{12-b}$$

Eq. (12-b) can be applied for all the internal nodes in the flow domain. A set of independent equations is found by applying Eq. (12-b) for all the nodes that can be solved by implementation of the known hydraulic head on the boundary nodes. To reach this goal, these equations are discretized according to the state of the nodes. The resulting procedure can be represented by matrix equation as

$$[D_{kf}]\{H_k\} + [D_{ff}]\{H_f\} = 0, \tag{13}$$

where the subscripts of k and f refer to constrained and free nodes (or boundary and internal nodes), with predefined and unknown hydraulic head values, respectively. H_f and H_k are the vectors containing the hydraulic head of internal and boundary nodes, respectively, D_{kf} is the asymmetric matrix of normalized conductance of the fracture segments between internal and boundary nodes, and D_{ff} is the asymmetric matrix of normalized conductance of the fracture segments between internal nodes. The matrix D_{kf} consists of n rows and m columns that are corresponded to the number of internal and boundary nodes, respectively, where the component in position i,j is d_{ij} of the fracture segment joining i-th boundary node and j-th internal node or is zero if they are not connected. The D_{ff} is an asymmetric square matrix that contains n rows and columns, where all the diagonal components of this matrix have the value of -1, and the off-diagonal component in position i,j is d_{ji} of fracture segment (starting from j-th internal node) meeting the i-th internal node or is zero if they are not connected.

Eq. (13) is solved through a numerical scheme with respect to the appropriate boundary conditions coming from the known hydraulic head on the boundary nodes. For both the internal and external boundary nodes, the prescribe pressure head, or free flow, hydraulic boundary condition was imposed in the numerical analysis. The hydraulic head for internal boundary nodes is accompanied with elevation head and pressure head of the column of gas and oil. The hydraulic head on the external boundary nodes is calculated by summation of the pressure head of water curtain and elevation head.

3.3. Migration tracing of hydrocarbon

The hydraulic head of all fracture nodes in the flow domain is obtained by solving Eq. (13); while the occurrence of hydrocarbon migration through fractures in the flow domain can be calculated by using the hydraulic head of fracture nodes in the flow domain. For this purpose, a special algorithm, so-called “migration tracing” was developed based on the application of the migration cessation criterion (Eq. (7)) through pathway analysis in the flow domain. To apply this algorithm, it is necessary to define the main or initial migration source points. The main migration source points are defined as the intersection of fractures with storage cavern (the nodes on the cavern boundary) if there is special flow conditions. It should be noted that, all the hydraulically active fractures directly connected to the cavern are not the migration source points. Hence, a concept, so-called “kinematic state”, was developed to identify the migration source points. Based on the flow direction (through the fractures), three different kinematic states can be considered for the fractures directly intersecting the cavern (Fig. 4):

(I) The outward flow from inside the cavern to the surrounding rock.
(II) The simultaneous inward (from rock into the cavern) and downward flow (from the node with higher elevation to the node with lower elevation).
(III) The simultaneous inward and upward flow (from the node with lower elevation to node with higher elevation).

From the above conditions, the intersecting nodes of the fractures (connected to the cavern) with kinematic state (I) are the main migration source points. The hydrocarbon inside the cavern certainly migrates from this kind of fractures. For the fractures with kinematic state (II), the hydrocarbon migration occurs only if the migration cessation criterion (Eq. (7)) is not satisfied. Such nodes also appear as the main migration source points. Hydrocarbon migration is not expected for the fractures with kinematic state (III). In fact, the fractures with inward and upward flow direction are not the source point of hydrocarbon migration. After all the main source points of migration are identified, the pathway analysis will be executed.

For each main source points, a pathway network is defined as the cluster of interconnected fractures that are linked (directly or indirectly) to the main source point. A library of migrated fractures is formed for each main source points (Fig. 5). All the fractures pathway cluster through which the hydrocarbon migrates are

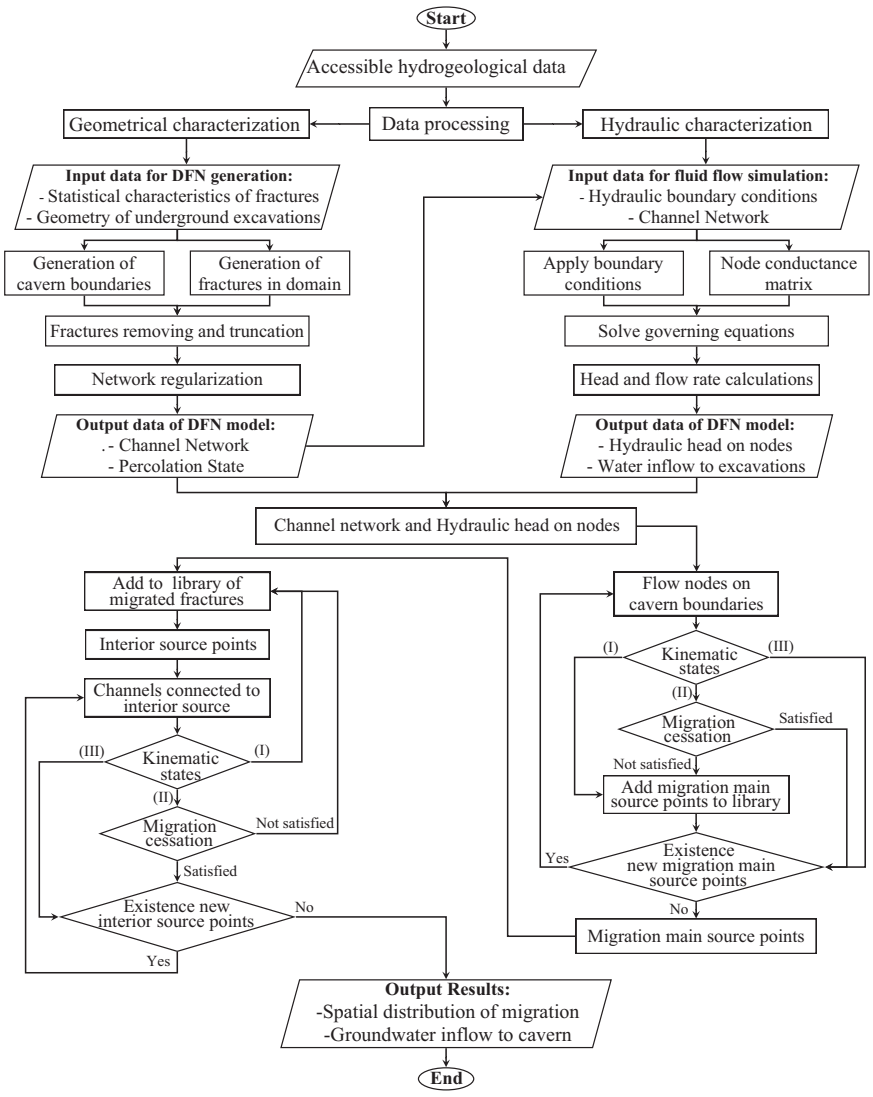

Fig. 5. The general algorithm for numerical modeling of discrete fluid flow analysis and hydrocarbon migration around unlined rock caverns.

stored in this library. The first member of this library is the fracture channel starting from the main source point. The second node on the channel starting from the main source point is considered as the interior source point. The kinematic states will be checked for all the fractures connected to the interior source points (except the channels stored in the migration library), the same as the method mentioned above. These channels are added to the library if the kinematic state and migration cessation criterion indicate the occurrence of migration. Similarly, the second node of these channels (added to the library) are considered as the new interior source points and the above pathway analysis will be repeated. This process will be continued until there is no new interior source point in the flow domain. The general algorithm of the developed numerical method for discontinuum modeling of hydrocarbon migration around the URCs is shown in Fig. 5.

4. MODEL SET-UP

In this study, the fluid flow analysis and hydrocarbon migration modeling were performed in two steps including the verification and application for DFN cases. For each of these purposes, similar numerical set-up and hydraulic boundary conditions were used in the fluid flow analysis. However, different discrete representations of fractured media around storage cavern were applied for the verification and application purposes.

A simple uniform discrete model of an artificial rock mass was used for verifying the developed method, and to evaluate the accuracy and the efficiency of numerical calculations. This discrete model involves two orthogonal conjugate persistent or infinite and equally spaced fracture sets (a vertical and a horizontal fracture sets) with constant spacing of 0.5 m and aperture of 100 μm. This discrete model was selected in such a way that the results of discrete calculations can be compared with the results of equivalent continuum representation. Considering the method proposed by Parsons (1966), the equivalent principal components of isotropic hydraulic conductivity tensor of this rock mass is calculated as 16.6×10^{-7} m/s. For verification purpose, the numerical fluid flow analysis was performed with both continuum and discontinuum methods by utilization of *Phase*^{2} finite element program and FNETF computational code, respectively.

A flow domain of 60 m width and 65 m height (Fig. 6) was used for fluid flow and hydrocarbon migration analysis, where the cavern with width of 20 m and height of 25 m is located in the middle of the domain. The minimum distance between the cavern roof and upper boundary of the flow domain is 20 m. The water curtain was considered to be located on the upper boundary of the flow domain. A fixed water bed with thickness of 0.5 m was

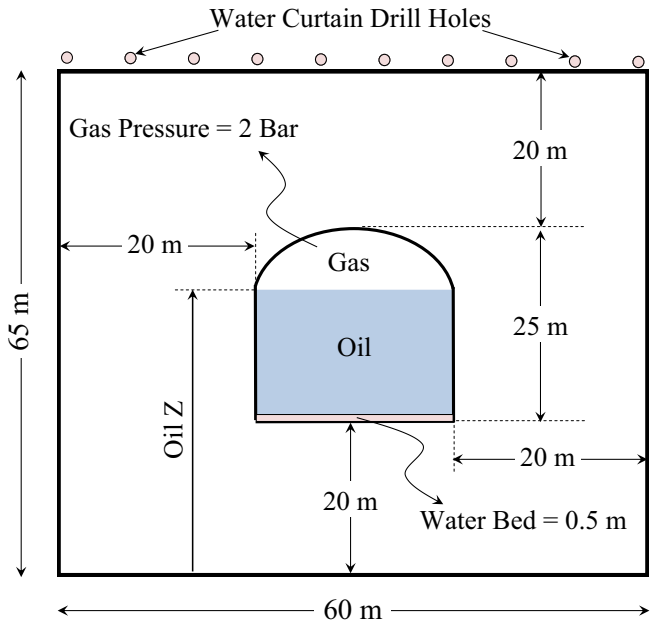

Fig. 6. Geometry of flow domain for fluid flow and hydrocarbon migration analysis.

designated below the oil in the cavern. All the fluid flow analyses were performed for pressurized unlined crude oil storage with fixed gas pressure of 2 bar and oil density of 900 kg/m^3. The hydraulic boundary conditions for external boundaries were assigned based on the pressure head of water curtain and elevation head of boundaries. The hydraulic head for internal boundaries was accompanied with elevation head and pressure head column of the gas and oil. The numerical modeling of fluid flow and hydrocarbon migration were performed for different hydraulic boundary conditions including three oil heights in the cavern (Oil Z) of 37.5, 40, and 42.5 m (from the bottom of the flow domain) and water curtain pressure heads (WCPH) of 0, 5, 10, 15, and 20 m.

In order to evaluate the applicability of the developed numerical method for naturally fractured rock mass, some results from hydrocarbon migration of DFN case examples are discussed in the second step. A similar numerical set-up of the verification case in terms of flow domain size, pressure of gas, and hydraulic boundary conditions was also utilized in this step. The main input data for generating DFN realizations consist of the geometrical properties of the fractures (such as orientation, trace length, and density) that were captured from real site investigations (Javadi and Sharifzadeh, 2011b). The geometrical properties of fractures that used in DFN generation are summarized in Table 1. Moreover, a constant hydraulic aperture of 100 μm was set for all the fractures in the flow domain.

Table 1
Geometrical properties of fractures for generation of DFN realizations.

Parameter	Fracture class			
	M1	M2	M3	RF
Fracture density (m^{-2})	0.207	0.129	0.063	0.144
Relative frequency	37.8	23.6	11.8	26.7
Dip/Dip direction	57/016	63/315	57/198	–*
Fisher constant	12.34	2.64	16.3	–*
Max. trace length (m)	12.5	11.5	12.2	12.5
Geometric mean of trace length (m)	2.55	2.55	2.77	2.73
Standard deviation of trace length	0.44	0.46	0.42	0.42

* For non-systematic class RF, orientation is assumed to be a stationary random function.

5. Results and discussion

5.1. Verification of numerical method

The output results of both continuum and discontinuum methods for the different hydraulic boundary conditions in terms of pressure head, hydraulic head, and the horizontal and vertical hydraulic gradient distributions around the cavern were found to match. Here, the simulation results of four different cases (hereafter called VC1, VC2, VC3, and VC4) were selected for verification of the developed method. The corresponding hydraulic boundary conditions in terms of (Oil Z,WCPH) for VC1, VC2, VC3, and VC4 were assigned as (37.5,0), (37.5,5), (40,10), and (42.5,15), respectively.

The simulation results of fluid flow and hydrocarbon migration for VC1 are compared in Fig. 7. The outputs of continuum analysis in terms of vertical and horizontal hydraulic gradient and flow direction around the cavern are shown in Fig. 7a–c, respectively. In Fig. 7d–f, the results of the discontinuum analysis with emphasis on the gas migration in the flow domain are shown. From the Eq. (7) and Åberg's criterion, the vertical hydraulic gradient greater than 1.0 should be maintained through the vertical fractures intersecting the cavern to eliminate the gas migration. Considering this critical value and definition of the hydraulic gradient in *Phase*^{2}, the distribution of the area around the cavern with gas migration potential (the colored area) is shown in Fig. 7a. All the colored area in Fig. 7a shows the downward flow (in the opposite direction of y) and equivalent kinematic state (II). The white zone on the top of the cavern indicated by UPF in Fig. 7a shows the upward flow or outward flow from the cavern (as shown in Fig. 7c) that equals the kinematic state (I). The distribution of the horizontal hydraulic gradient (Fig. 7b) indicates most area around the cavern where the groundwater continuously flows from outside rock toward the cavern. For the area above the cavern, the groundwater shows a divergent flow (i.e. flow direction from point O to points C and C′). This issue is also shown in Fig. 7c. The maximum width of divergent flow above the cavern (C–C′ in Fig. 7b) is about 25.6 m.

The arrangement of fractures migrated by gas from VC1 is shown in Fig. 7d. It can be observed that the gas migration occurs in both horizontal and vertical fractures around the cavern. The upper extension of the migrated fractures is limited to the upper boundary of flow domain. The lower extension of migrated fractures is limited to the cavern roof or an arc-type area near the cavern floor (DML in Fig. 7d). From the results of continuum fluid flow analysis (Fig. 7a–c), the gas migration occurs in all the vertical fractures intersecting the cavern roof that is also predicted in the results of the migration analysis with FNETF. The upper extension of the migrated fractures also matched the results of the continuum fluid flow analysis, where the vertical hydraulic gradient for all the area between the cavern roof and upper boundary of flow domain is lower than the critical value.

As shown in Fig. 7d, the migrated zone with a width of 25.5 m (A–A′) is laterally extended from the vertical walls of the cavern, where the horizontal length of A–A′ is very close to the width of divergent flow above the cavern or C–C′ in Fig. 7b. In fact, the lateral extension of migrated zone is controlled by gas migration in the horizontal fractures. Theoretically speaking, the hydrocarbon migration in horizontal fractures around the cavern only occurs for outward flow or in the case of kinematic state (I). In order to show the lateral extension of gas migration, the result of discontinuum fluid flow simulation and migration analysis in the fracture network located in Zone R1 (as defined in Fig. 7a) is shown in Fig. 7e. The gas migrated zone (highlighted area) and flow direction in the fractures are shown in Fig. 7e. Moreover, some of the intersection points of the fractures are selected in the Zone R1 to visually

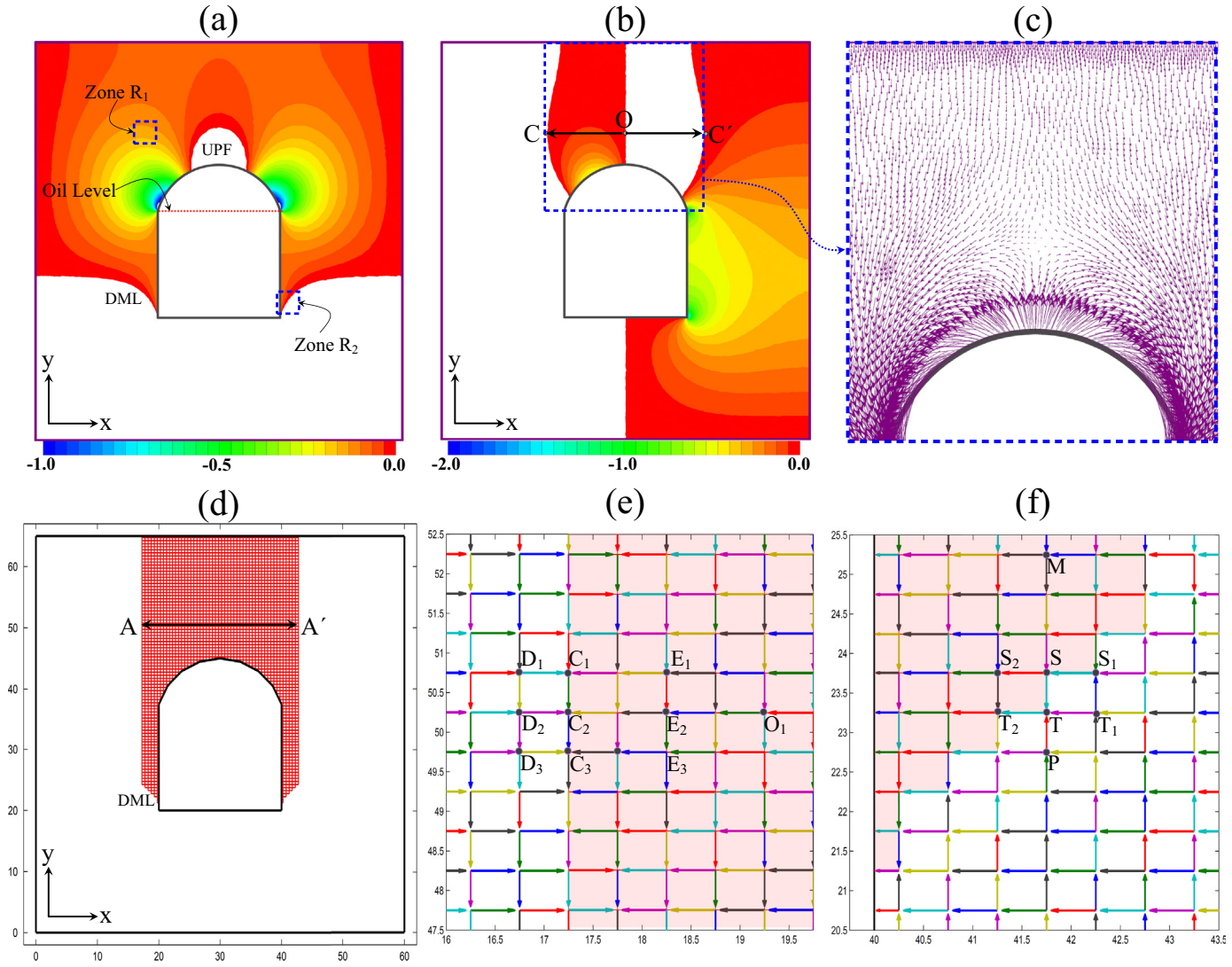

Fig. 7. Results of fluid flow and hydrocarbon migration using continuum and discontinuum analyses for VC1: (a) distribution of vertical hydraulic gradient, (b) distribution of horizontal hydraulic gradient, (c) distribution of flow velocity vector, (d) gas migrated fractures, (e) flow direction in the fracture network located in the Zone R1, and (f) flow direction in the fracture network located in the Zone R2.

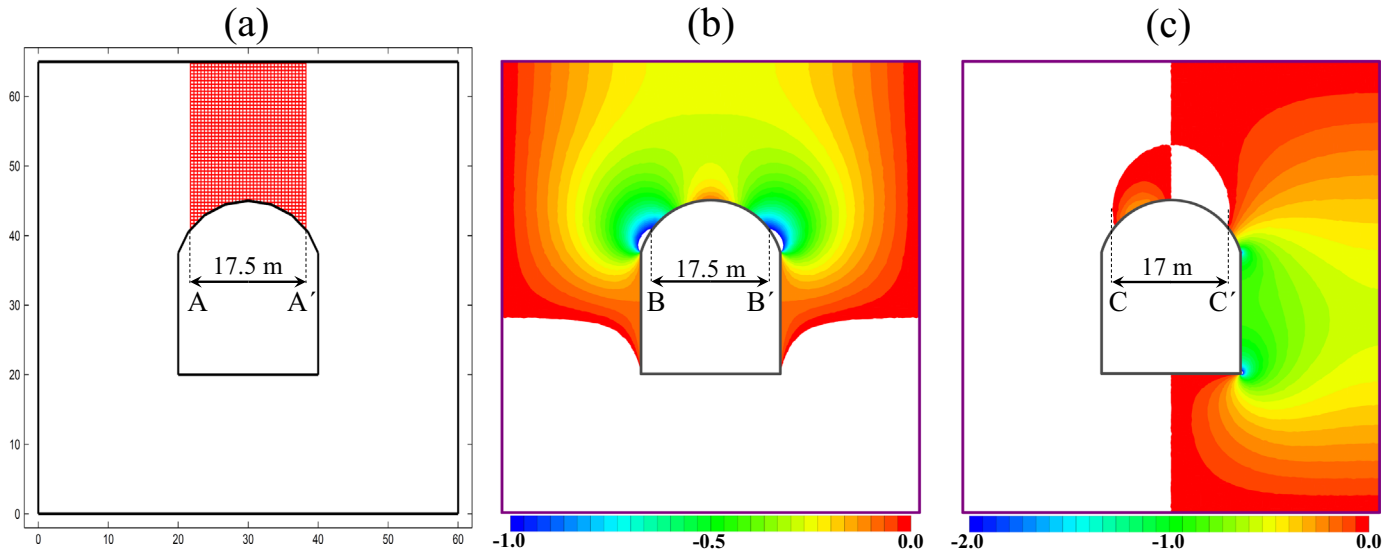

Fig. 8. Results of fluid flow and hydrocarbon migration analyses for VC2: (a) gas migrated fractures, (b) distribution of vertical hydraulic gradient, and (c) distribution of horizontal hydraulic gradient.

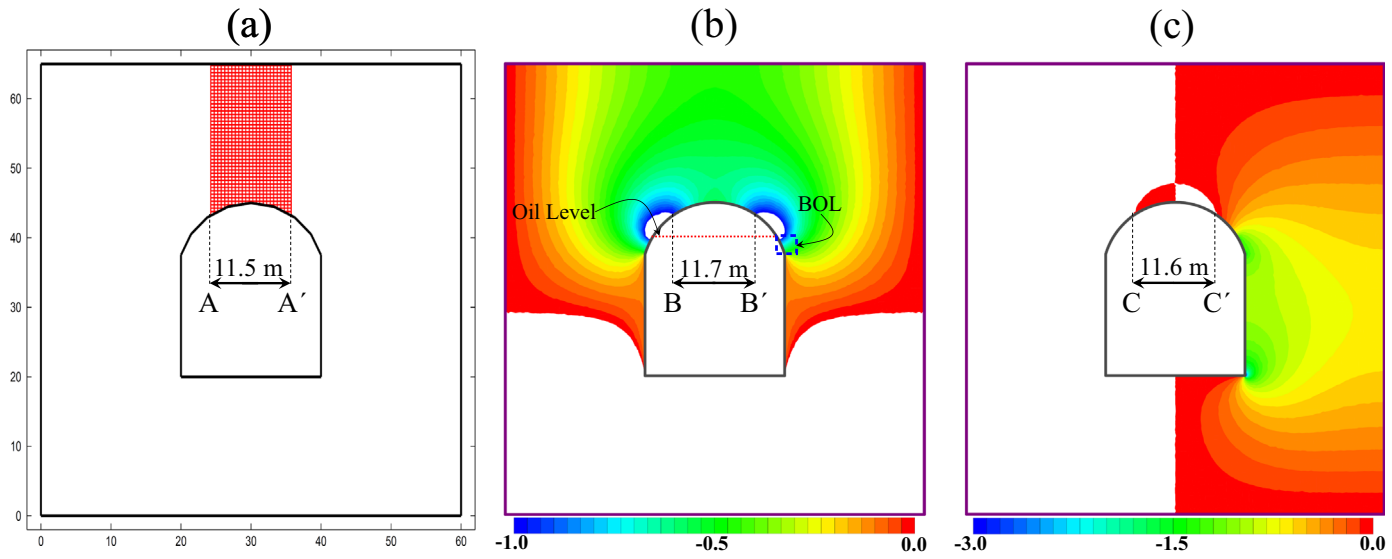

Fig. 9. Results of fluid flow and hydrocarbon migration analyses for VC3: (a) gas migrated fractures, (b) distribution of vertical hydraulic gradient, and (c) distribution of horizontal hydraulic gradient.

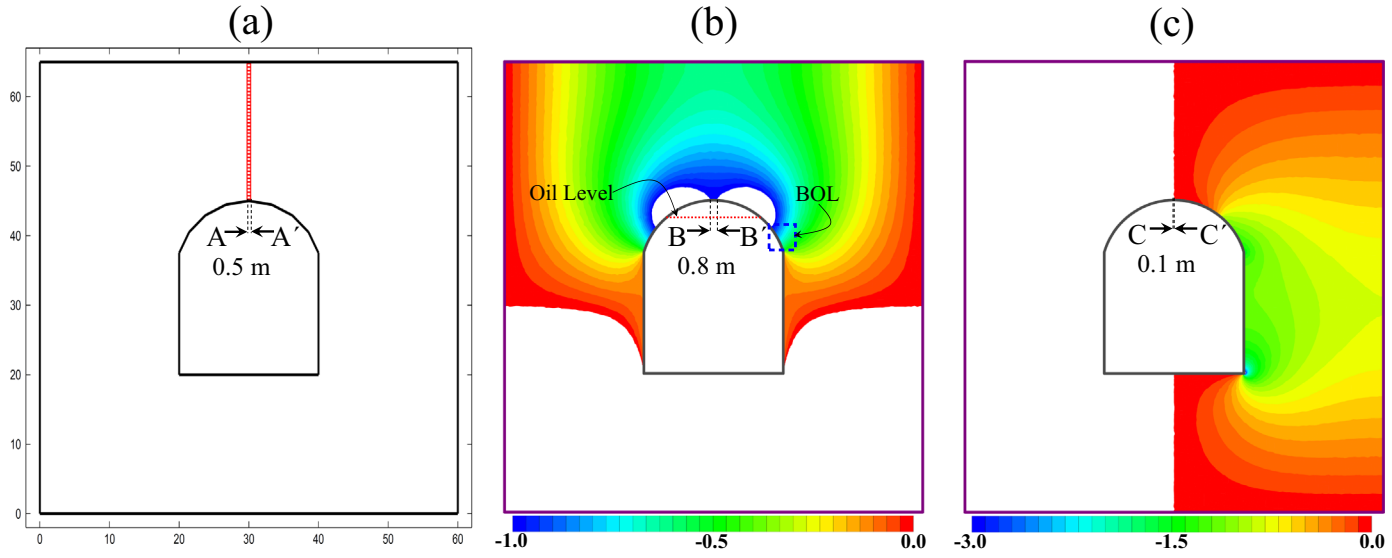

Fig. 10. Results of fluid flow and hydrocarbon migration analyses for VC4: (a) gas migrated fractures, (b) distribution of vertical hydraulic gradient, and (c) distribution of horizontal hydraulic gradient.

describe the migration process in the fracture network. The point O1 is considered as the initial interior migration source point in the Zone R1, where this point has been migrated due to the gas migration in the fractures above the cavern. The gas starts to migrate from O1 to E2, due to the outward flow from O1 to E2 or equivalent kinematic state (I). Since the vertical hydraulic gradient for the fracture between E1 and E2 is lower than the critical value, the gas migration occurs from E2 to E1. This upward gas migration continues for all the vertical fractures from E1 or E2 to the upper boundary of the flow domain. Part of the gas migration in E3 supplies with the outward flow from E2 to E3. This downward gas migration also continues for all the vertical fractures from the E3 to the DML area. Similar gas migration process exists for C1, C2, and C3. The horizontal gas migration ceases in C1, C2, and C3 due to the change in horizontal flow direction in these points. In fact, the divergent or outward flow condition disappears in C1, C2, and C3 and therefore horizontal gas migration can not be continued in these points.

The gas migrated zone and flow direction in the fracture network located in the Zone R2 are shown in Fig. 7f. This figure illustrates how the gas migration breaks off in the DML area. The point M is considered as the initial interior migration source point in the Zone R2, where this point has been migrated due to the gas migration in fractures near the point C′ in Fig. 7b or the equivalent E1 point corresponding to the symmetric plan of flow domain. The gas starts the downward migration from M to S, due to the outward flow from M to S or equivalent kinematic state (I). In addition, part of gas migration in S supplies with the outward flow from S1. Same migration process can be considered for S1 and S2 points. The downward migration form S continues until the gas receives the point T. The downward migration ceases in point T due to the change in vertical flow direction at this point. The gas migrating from T is directed to the T2 as shown by the flow direction in the fracture between these points. However, no horizontal gas migration occurs between the points T and T1 because the flow is directed from T1 to T. In addition, the gas migration is impossible in the vertical fracture between the points T and P, since the flow in this fracture is upward with equivalent kinematic state (III).

The results of fluid flow and hydrocarbon migration analyses

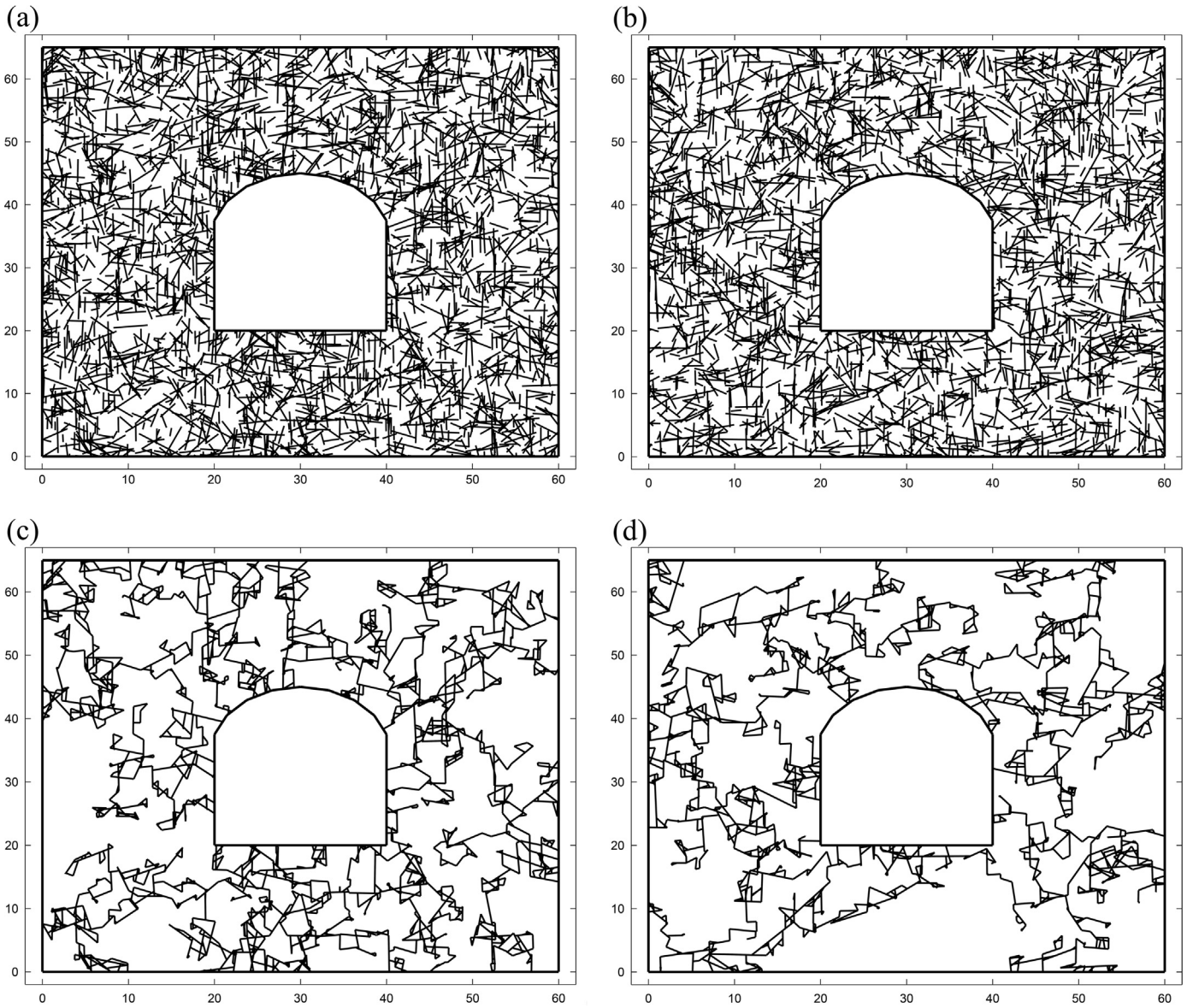

Fig. 11. Graphical representation of two generic examples for migration analysis: (a) first DFN realization, (b) second DFN realization, (c) the regularized channel network for first DFN realization, (d) regularized channel network for second DFN realization.

for VC2, VC3, and VC4 are respectively shown in Figs. 8–10. In Figs. 8–10, the width of migrated zone of fractures, the width of area with gas migration potential or vertical hydraulic gradient lower than the critical value for gas migration, and the maximum width of divergent flow above the cavern were indicated as A–A′, B–B′, and C–C′, respectively. The length of A–A′, B–B′, and C–C′ for VC2, VC3, and VC4 are 17.5, 11.5, and 0.5 m, 17.5, 11.7, and 0.8 m, and 17, 11.6, and 0.1 m, respectively. For all of these cases, unlike the VC1, the maximum width of divergent flow above the cavern is lower than the width of area with vertical gas migration potential. Therefore, for these cases, the gas migration in the fractures network around the cavern is controlled by the width of the area with vertical gas migration potential. For these cases, there is a good corresponding between the lengths of A–A′ and B–B′, where the difference between the widths of area with vertical gas migration potential and migrated zone of fractures is lower than the fracture spacing. In addition, the upper extension of the migrated fractures (in Figs. 8a, 9a, and 10a) matches with the results of continuum fluid flow analysis, where the vertical hydraulic gradient for all the area between the cavern roof and upper boundary of flow domain (in Figs. 8b, 8b, and 10b) is lower than the critical value. For VC3 and VC4, there are some areas above the cavern roof that show vertical gas migration potential but no hydrocarbon migration occurs in such zones. These zones were indicated as BOL in Figs. 9b and 10b. The main reason of this issue is that these area are located below the oil level in the cavern and therefore no gas migration occurs. In addition, the vertical hydraulic gradient in these area is more than the critical value of 0.1 (as calculated with Eq. (7) for oil with density of 900 kg/m^3) and as a result, the oil migration is impossible for BOL zones.

Comparison of these results indicates that there is an acceptable coincidence between the prediction of hydrocarbon migration in discrete fracture model and the results of fluid flow analysis in continuum model. For all the selected cases for verification (VC1, VC2, VC3, and VC4), the lateral extension of migrated fractures around the cavern matches the length of area with gas migration potential (with vertical hydraulic gradient lower than the critical value) or maximum width of divergent flow above the cavern. In addition, for all the verification cases, the vertical extension of migrated fractures around the cavern matches the

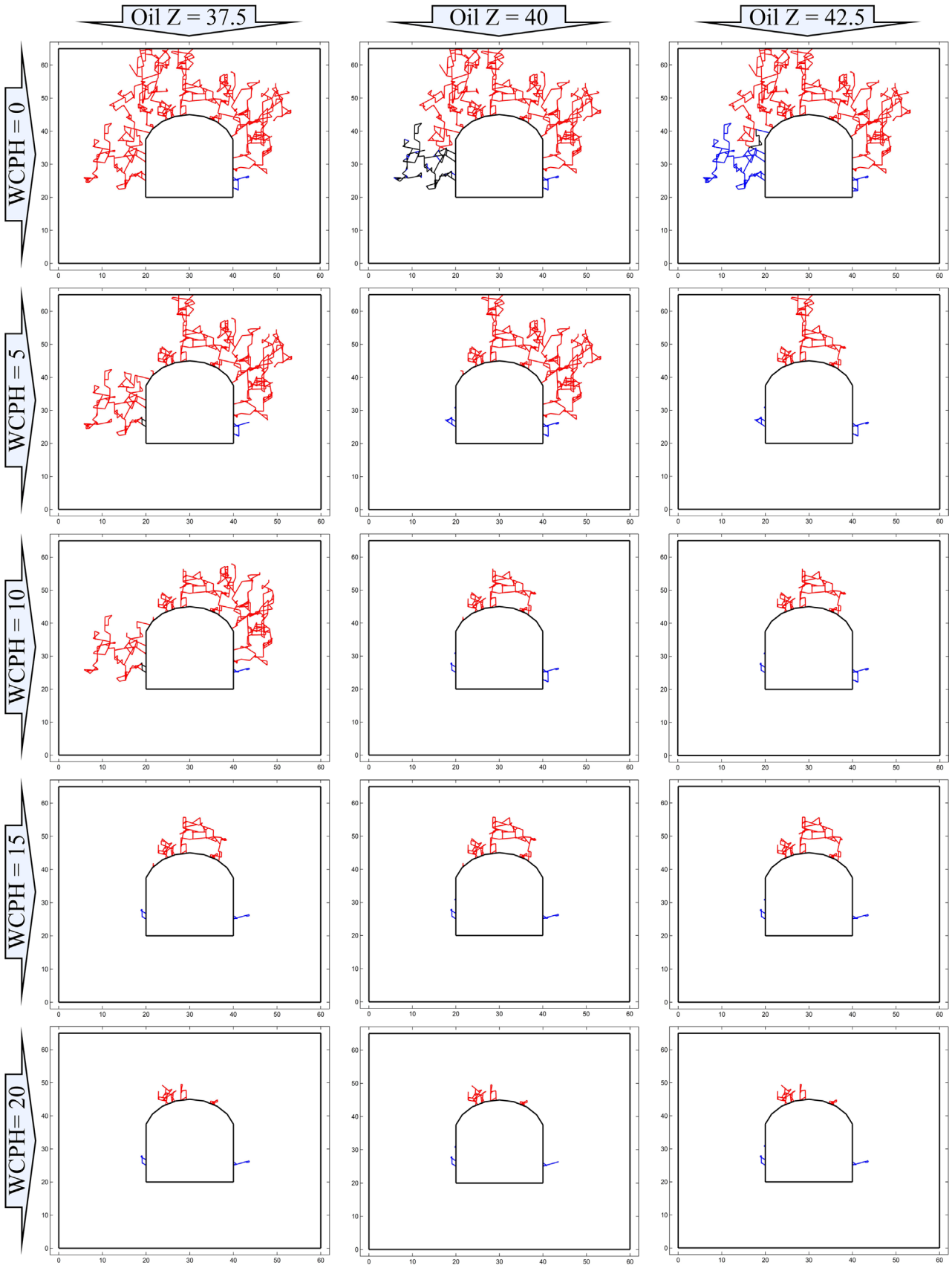

Fig. 12. Effect of hydraulic boundary conditions on the hydrocarbon migration around the cavern for CI. The water curtain pressure (WCPH) increases from top to down and the height of oil in the cavern (Oil Z) increases from left to right side (Blue: oil migrated fractures, Red: gas migrated fractures, Black: both oil and gas migrated fractures). (For interpretation of the references to color in this figure legend, the reader is referred to the web version of this article.)

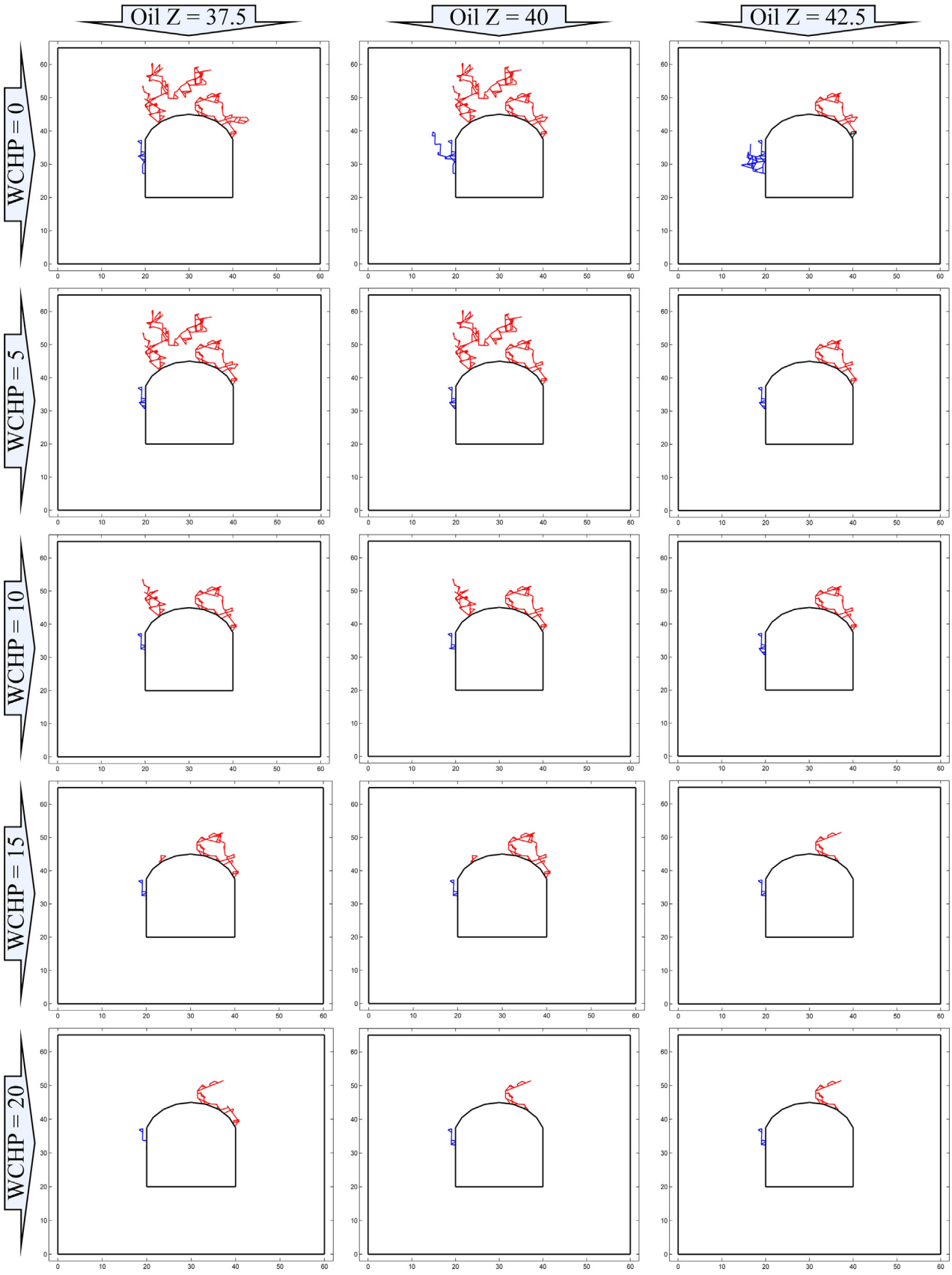

Fig. 13. Effect of hydraulic boundary conditions on the hydrocarbon migration around the cavern for CII. The water curtain pressure (WCPH) increases from top to down and the height of oil in the cavern (Oil Z) increases from left to right side (Blue: oil migrated fractures, Red: gas migrated fractures, Black: both oil and gas migrated fractures). (For interpretation of the references to color in this figure legend, the reader is referred to the web version of this article.)

critical vertical hydraulic gradient for gas migration or the flow direction.

5.2. Application of hydrocarbon migration analysis for DFN examples

In order to evaluate the applicability of developed numerical method for naturally fractured rock mass, the results of hydrocarbon migration in two different arbitrary DFN realizations with same input data of geometrical properties of fractures are presented in this section. These two DFN realizations with their regularized channel network are shown in Fig. 11. As shown in Fig. 11, only a few generated fractures in the flow domain are hydraulically active. The regularized channel networks were used for fluid flow modeling and hydrocarbon migration analysis. The results of the hydrocarbon migration analysis for these DFN realizations are shown in Figs. 12 and 13. In both of these figures, the water pressure on the external boundaries or WCPH increases from top to down. Moreover, the height of oil in the cavern (from the bottom of the domain) is shown by "Oil Z" that increases from left to right. The hydrocarbon tracing was performed for oil and gas migration, where the migrated fractures are shown in blue and red colors, respectively. The black color fractures in Figs. 12 and 13 represent the migration of both oil and gas.

Figs. 12 and 13 visually present how hydraulic boundary conditions affect the hydrocarbon migration in the fractures surrounding the cavern. Generally, the number of migrated fractures with oil (blue lines) and gas (red lines) increases and decreases, respectively, as the height of oil in the cavern rises. In both DFN realizations, the number of migrated fractures with gas is much larger than oil. The number of migrated fractures generally decreases by increasing the WCPH; however, the effects of external water pressure on the number of migrated fractures are different for these DFN realizations.

In the first DFN realization (Fig. 12), the hydrocarbon migration is very sensitive to the hydraulic boundary conditions. For zero WCPH, by increasing the Oil Z, the number of migrated fractures with oil and gas obviously increases and decreases respectively. However, the number of total migrated fractures does not show meaningful variation. The reduction of gas migrated fractures will be more apparent for the case with WCPH of 5 m. Similar variations can be also observed for the case with WCPH of 10 m, but the gas migrated fractures show smaller reduction by increasing the Oil Z from 40 m to 42.5 m. For more WCPHs (15 m and 20 m), the Oil Z does not distinctly influence the hydrocarbon migration, where the number of migrated fractures remains more constant. In the cases of small WCPHs (zero and 5 m), the gas migrates in long distances from the cavern. For these cases, there is a network of gas migrated fractures that connects the cavern to the upper external boundary of the flow domain. In such situation, the gas can be leaked out from the flow domain. This issue refers to a phenomenon called "gas escape" that becomes extinct by increasing the WCPH.

The hydrocarbon migration in the second DFN realization shows less sensitivity to the hydraulic boundary conditions. The migration distance from the cavern is shorter than first DFN realization, and gas escape phenomenon do not occur. Moreover, the reduction in the migration distance by increasing the WCPH is much less than the first DFN realization. The migration distance decreases effectively by increasing the WCPH to 5 m. However, by increasing the WCPH from 10 to 20 m, a small decrease in the migration distance of hydrocarbon was indicated in the results. For the cases with zero and 5 m water curtain pressure heads, the number of gas migrated fractures decreases by increasing the height of oil in the cavern, especially for Oil Z of 42.5 m. The reverse behavior can also be observed for the number of oil migrated fractures. In addition, by increasing the Oil Z, the total number of migrated fractures decreases for all the cases.

6. Conclusion

In this paper, a numerical method was developed for modeling of hydrocarbon migration around the unlined rock caverns based on the direct utilization of DFN concept. To reach this goal, an algorithm including new concepts such as "migration tracing" and "kinematic state" was developed based on the pathway analysis in the DFN and applying the migration cessation criterion.

The accuracy of the developed numerical method was explored by predicting the hydrocarbon migration in a uniform fracture network around an unlined cavern and comparing the results with that of finite element continuum fluid flow analysis. Finally, the hydrocarbon migration was simulated in DFN realizations to present how the pressure of water curtain and height of oil in the cavern affect the migration circumstance in naturally fractured rock mass. Based on the results presented, the following conclusions were obtained:

- The host rock mass for unlined hydrocarbon storages are usually hard and massive with few discontinuities, where the influence of fractures on groundwater flow and hydrocarbon migration cannot be neglected. Since DFN concept explicitly reflects the dominance of fractures geometry in hydraulic processes, this concept is more consistent for fluid flow and migration analysis in the rock mass surrounding the storage caverns, especially for the near-field applications.
- The hydrocarbon migration can be practically controlled by establishing sufficient water pressure in the fracture system that is provided by water curtain in most of the cases. The results indicate that the number of migrated fractures generally decreases by increasing the pressure of water curtain; however, the effects of external water pressure on the number of migrated fractures are highly dependent on the fractures geometry and height of oil in the cavern. The hydrocarbon migration was found to be very sensitive to geometrical arrangement of fractures and as a consequence, local migration paths may develop around storage cavern through the intricately connected fracture network, despite the presence of high pressurized water curtain.
- With sufficient information of fractures geometry and hydraulic conditions, the developed methodology can be applied to model fluid flow and hydrocarbon migration through the interconnected fractures around the URCs. Through this application, a better understanding can be reached for the fluid flow processes that take place in the complex domain of naturally fractured rocks around storage cavern.

References

Åberg, B., 1977. Prevention of gas leakage from unlined reservation in rocks. Paper presented at First International Symposium on Storage in Excavated Rock Cavern, Rock Store 77, Stockholm, Sweden.

Aoki K., Ismail A., Uno H., Chang C.S., Maejima T., Nakamura K., 2010. Hydraulic behaviors characterization for the design of unlined underground LPG storage cavern in fractured rock mass. Paper presented at ISRM International Symposium, EUROCK 2010, Lausanne, Switzerland.

Chung, I.M., Cho, W., Heo, J.-H., 2003. Stochastic hydraulic safety factor for gas containment in underground storage caverns. J. Hydrol. 284 (1–4), 77–91. http://dx.doi.org/10.1016/S0022-1694(03)00275-0.

Dershowitz W.S., Lapointe P., 1995. Discrete fracture hydrogeology for underground storage caverns. Paper Presented at 8th ISRM Congress, Tokyo, Japan.

Froise, S., 1987. Hydrocarbon storage in unlined rock caverns: Norway's use and experience. Tunn. Undergr. Space Technol. 2 (3), 265–268. http://dx.doi.org/10.1016/0886-7798(87)90033-2.

Goel, R.K., Singh, B., Zhao, J., 2012. Underground Infrastructures. Elsevier, Waltham.

Goodall, D.C., Åberg, B., Brekke, T.L., 1988. Fundamentals of gas containment in unlined rock caverns. Rock. Mech. Rock. Eng. 21 (4), 235–258. http://dx.doi.org/

10.1007/BF01020278.
Indraratna, B., Ranjith, P.G., Gale, W., 1999. Single phase water flow through rock fractures. Geotech. Geol. Eng. 17, 211–240.
Indraratna, B., Ranjith, P., Price, J., Gale, W., 2003. Two-phase (air and water) flow through rock joints: analytical and experimental study. J. Geotech. Geoenviron. Eng. 129 (10), 918–928.
Javadi, M., Sharifzadeh, M., 2014. Fluid flow modeling in discontinuous rock media using a distinct fracture network. Sharif J. Sci. Technol. Civil. Eng. 2–30 (3), 107–116.
Javadi, M., Sharifzadeh, M., Shahriar, K., 2010. A new geometrical model for non-linear fluid flow through rough fractures. J. Hydrol. 389 (1–2), 18–30. http://dx.doi.org/10.1016/j.jhydrol.2010.05.010.
Javadi, M., Sharifzadeh, M., Shahriar, K., 2016. Uncertainty analysis of groundwater inflow into underground excavations by stochastic discontinuum method: case study of Siah Bisheh pumped storage project, Iran. Tunn. Underg. Space Technol. 51, 424–438. http://dx.doi.org/10.1016/j.tust.2015.09.003.
Javadi, M., Sharifzadeh, M., Shahriar, K., Mitani, Y., 2014. Critical Reynolds number for nonlinear flow through rough-walled fractures: The role of shear processes. Water Resour. Res. 50, 1789–1804. http://dx.doi.org/10.1002/2013WR014610.
Javadi M., Sharifzadeh M., 2011a. Modeling Of Fluid Flow In Rock Mass Using Distinct Fracture Network Concept With Emphasis on FNETF Computational Code Development. Paper Published at 4th Iranian Rock Mechanics Conference (IRMC4), Tehran, Iran, pp. 35–40.
Javadi M., Sharifzadeh M., 2011b. Assessment of inflow possibility into underground excavation using DFN and percolation concepts. Paper Published at 22nd World Mining Congress, Turkey. Volume IV, pp. 3–10.
Kim, J., Cho, W., Chung, I.-M., Heo, J.-H., 2007. On the stochastic simulation procedure of estimating critical hydraulic gradient for gas storage in unlined rock caverns. Geosci. J. 11 (3), 249–258. http://dx.doi.org/10.1007/BF02913938.
Kim, T., Lee, K.-K., Ko, K.S., Chang, H.W., 2000. Groundwater flow system inferred from hydraulic stresses and heads at an underground LPG storage cavern site. J. Hydrol. 236, 165–184.
Kjørholt, H., Broch, E., 1992. The water curtain-a successful means of preventing gas leakage from high-pressure, unlined rock caverns. Tunn. Undergr. Space Technol. 7 (2), 127–132. http://dx.doi.org/10.1016/0886-7798(92)90042-G.
Lee, C.-I., Song, J.-J., 2003. Rock engineering in underground energy storage in Korea. Tunn. Undergr. Space Technol. 18 (5), 467–483. http://dx.doi.org/10.1016/S0886-7798(03)00046-4.
Liang, J., Lindblom, U., 1994. Analyses of gas storage capacity in unlined rock caverns. Rock. Mech. Rock. Eng. 27 (3), 115–134. http://dx.doi.org/10.1007/BF01020306.
Lindblom, U.E., 1997. Design criteria for the Brooklyn Union Gas storage caverns at JFK airport New York. Int. J. Rock. Mech. Min. Sci. 34 (3–4), 179.e1–179.e16. http://dx.doi.org/10.1016/S1365-1609(97)00040-3.
Lu, M., 2010. Rock engineering problems related to underground hydrocarbon storage. J. Rock. Mech. Geotech. Eng. 2 (4), 289–297. http://dx.doi.org/10.3724/SP.J.1235.2010.00289.
Maejima T., Uno H., Mito Y., Chang C.S., Aoki K., 2007. Three-dimensional hydro-geological modelling around the large rock cavern for the LPG storage project. Paper presented at 11th ISRM Congress, Lisbon, Portugal.
Parsons, R.W., 1966. Permeability of idealized fractured rock. Soc. Pet. Eng. J. 6, 126–136.
Priest, S.D., 1993. Discontinuity Analysis of Rock Engineering. Chapman & Hall, London.
Ra, S.H., Sung, W.M., 1999. An analysis of gas tightness around unlined storage cavern using a discrete fracture flow FEM model. Geosystem Eng. 2 (2), 61–67. http://dx.doi.org/10.1080/12269328.1999.10541142.
Renshaw, C.E., 1995. On the relationship between mechanical and hydraulic apertures in rough-walled fractures. J. Geophys. Res. 100 (B12), 629–636. http://dx.doi.org/10.1029/95JB02159.
Söder, C-O., 1995. Water curtains in gas storage- An experimental study. Paper presented at 8th ISRM Congress, Tokyo, Japan.
Sharifzadeh M., Javadi M., 2011. Near-field application of aperture back calibrated distinct fracture network. Paper published at 12th International Congress on Rock Mechanics (ISRM), Beijing, China, pp. 1361–1365.
Sun, J., Zhao, Z., 2010. Effects of anisotropic permeability of fractured rock masses on underground oil storage caverns. Tunn. Undergr. Space Technol. 25 (5), 629–637. http://dx.doi.org/10.1016/j.tust.2010.04.009.
Thunvik, R., Braester, C., 1981. Methods of confining oil in unlined caverns in aquifers: water table maintenance by well recharge. Water Resour. Res. 17 (1), 228–232. http://dx.doi.org/10.1029/WR017i001p00228.
Witherspoon, P.A., Wang, J.S.Y., Iwai, K., Gale, J.E., 1980. Validity of cubic law for fluid flow in a deformable rock fracture. Water Resour. Res. 16 (6), 1016–1024. http://dx.doi.org/10.1029/WR016i006p01016.
Yoshida, H., Maejima, T., Nakajima, S., Nakamura, Y., Yoshida, S., 2013. Features of fractures forming flow paths in granitic rock at an LPG storage site in the orogenic field of Japan. Eng. Geol. 152 (1), 77–86. http://dx.doi.org/10.1016/j.enggeo.2012.10.007.
Zhao, J., 1996. Construction and utilization of rock caverns in Singapore part a: the bukit timah granite bedrock resource. Tunn. Undergr. Space Technol. 11 (1), 65–72. http://dx.doi.org/10.1016/0886-7798(96)00054-5.